Analysis of Termination Impedance Effects on the Linearity of 5 GHz CMOS Radio Frequency Amplifiers

John S. Fairbanks *Student Member, IEEE*, and Lawrence E. Larson *Fellow, IEEE*
Electrical and Computer Engineering Department,
University of California, San Diego (UCSD), La Jolla, California, USA.
E-mail: jfairban@ece.ucsd.edu
WWW: http://www.cwc.edu

Abstract — **The high-frequency nonlinear distortion of a small-signal CMOS common-source amplifier stage is analyzed as a function of bias and termination impedance at 5 GHz. The results developed can be applied to wireless RF circuit design applications.**

I. Introduction

Portable, wireless, personal-communication devices continue to gain in popularity, and CMOS technology is becoming increasingly popular for the realization of key radio frequency components [1–3]. Although the intrinsic speed of scaled MOS devices is impressive, the use of CMOS devices for high-frequency applications has been limited by the digital orientation of the design and modelling environment. In particular, the optimum scaling, biasing, and tuning of the devices for the realization of the best high-frequency performance in a wireless environment remains a challenge [4].

Historically, there has been little work done on predicting optimum source and load impedances for maximizing linearity performance in MOSFET RF circuits. The purpose of this work is to develop some straightforward guidelines for optimizing the linearity of the monolithic common-source MOS amplifier in Fig. 1 for RF LNA, variable gain amplifier (VGA), and mixer applications in a wireless transceiver, *under the constraint of minimizing dc power dissipation*, by optimizing both the source and load termination impedances for optimum linearity.

II. Nonlinear MOSFET Transfer Function

A. Open Loop Analysis

Intermodulation distortion is the key limitation on the dynamic range performance, and our goal is to predict the nonlinear behavior, particularly third-order intermodulation, as a function of device design, biasing, and impedance termination [5,6].

A small-signal nonlinear model of the MOS transistor, is shown in Fig. 1. In the saturation region, the major sources of nonlinearity are the transconductance (g_m), the gate-source capacitance (C_{gs}), the channel resistance (r_o) and drain-substrate capacitance (C_{ds}) [7]. The gate-drain capacitance (C_{gd}) can be considered to be a linear element. The transistor transconductance can be characterized by a nonlinearity of the following general form [5]

$$i_{gm} = a_1 * v_{gs} + a_2 * v_{gs}^2 + a_3 * v_{gs}^3 + ... \quad (1)$$

where i_{gm} is the small-signal transconductance current

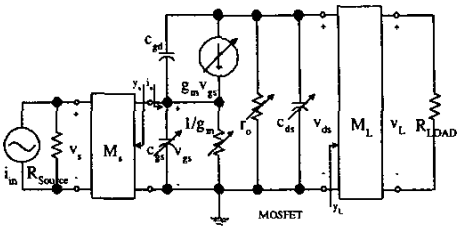

Fig. 1: Simplified small-signal MOSFET model equivalent circuit showing sources of nonlinear distortion.

and v_{gs} is the small-signal input voltage. Similarly, the output conductance can be characterized by the current through the channel [7] and

$$i_{ro} = g_1 * v_{ds} + g_2 * v_{ds}^2 + g_3 * v_{ds}^3 + ... \quad (2)$$

where the v_{gs} dependence on g_n is very small and does not have to be considered [7]. The output capacitor current can be modelled by

$$i_{c_{ds}} = c_1 \frac{dv_{ds}}{dt} + \frac{c_2}{2}\frac{dv_{ds}^2}{dt} + \frac{c_3}{3}\frac{dv_{ds}^3}{dt} + ... \quad (3)$$

and the input capacitor current can be modelled by

$$i_{c_{gs}} = c_{g1}\frac{dv_{gs}}{dt} + \frac{c_{g2}}{2}\frac{dv_{gs}^2}{dt} + \frac{c_{g3}}{3}\frac{dv_{gs}^3}{dt} \quad (4)$$

These coefficients can be measured, or derived from equivalent circuit model parameters.

Now, using the Volterra formalism for the output voltage in terms of the input voltage at the gate yields

$$v_{ds} = H_1 \circ v_{gs} + H_2 \circ v_{gs}^2 + H_3 \circ v_{gs}^3 + ... \quad (5)$$

and, using the Volterra series for the gate voltage in terms of the source current yields

$$v_{gs} = G_1 \circ i_s + G_2 \circ i_s^2 + G_3 \circ i_s^3 \quad (6)$$

Now, the total transfer function K without including the feedback effect due to C_{gd} is the product of the two transfer functions H and G. So

$$\begin{aligned} v_{ds} = {} & H_1 \circ \{G_1 \circ i_s + G_2 \circ i_s^2 + G_3 \circ i_s^3\} + \\ & H_2 \circ \{G_1 \circ i_s + G_2 \circ i_s^2 + G_3 \circ i_s^3\}^2 + \\ & H_3 \circ \{G_1 \circ i_s + G_2 \circ i_s^2 + G_3 \circ i_s^3\}^3 \end{aligned} \quad (7)$$

0-7803-7787-7/03/$17.00 © 2003 IEEE

or more compactly

$$v_{ds} = K_1 \circ i_s + K_2 \circ i_s^2 + K_3 \circ i_s^3 + \cdots \quad (8)$$

Next, the extensive definition of supporting terms is presented, from which are constructed the K_1, K_2, and K_3 :

From the above definitions, K_1, K_2, and K_3 Volterra kernels are constructed to predict two-tone intermodulation performance as shown next.

$$K_1(j\omega_1) = \frac{a_1}{A * F} \quad (9)$$

where

$A = \{g_1 + y_L(\omega_1) + j\omega_1 c_1\}$ and $F = \{y_s(\omega_1) + j\omega_1 c_{g1}\}$.

Next, the second order Volterra kernel is derived to the following:

$$K_2(\omega_1, \omega_1) = \left[\frac{\left[\{a_1\} j\omega_1 c_{g_2} \quad \{a_2\} + \frac{I_1}{A^2}\right] * E}{H * E * F^2} \right] \quad (10)$$

(11)

where

$E = \{2j\omega_1 c_{g1} + y_s(2\omega_1)\}$, $H = \{g_1 + y_L(2\omega_1) + 2j\omega_1 c_1\}$, and $I_1 = a_1^2 \{g_2 + j\omega_1 c_2\}$.

Finally, the third-order Volterra kernel is expressed in the following three parts:

$$K_3(j\omega_1, j\omega_1, \quad j\omega_2) = K_{3a} + K_{3b} + K_{3c} \quad (12)$$

where

$$K_{3a} = \left\{ \frac{a_1}{A} \right\} \left\{ \frac{B + C}{D \times E \times F^3} \right\} \quad (13)$$

with

$B = \frac{1}{3}(j\omega_1 c_{g2})^2$, $C = \left\{\frac{1}{3} j\omega_1 c_{g3}\right\} \{2j\omega_1 c_{g1} + y_s(2\omega_1)\}$, and $D = \{y_s(\ \omega_2) \quad j\omega_1 c_{g1}\}$.

Next,

$$K_{3b} = \left[\begin{array}{l} \frac{2}{3} \left\{ \frac{a_2 \times G \times H + a_1^2 \times I}{H \times A \times G} \right\} \left\{ \frac{1}{D} \right\} * \\ \left\{ \frac{j\omega_1 c_{g2}}{E \times K^2} \right\} \end{array} \right] \quad (14)$$

where

$G = \{g_1 + y_L(\ \omega_2) \quad j\omega_1 c_1\}$, $I = a_1^2 \{g_2 + \frac{1}{2} j\omega_1 c_1\}$, and $K = \{y_s \omega_1 + j\omega_1 c_{g1}\}$.

Lastly,

$$K_{3c} = \frac{1}{A} \left\langle a_3 + \left[\begin{array}{l} L \times \frac{1}{3} \times (2 \left\{ \frac{a_1}{A} \right\} \\ \left\{ \frac{a_2 \times A \times G + a_1^2 \times g_2}{g_1 \times A^2} \right\} \end{array} \right] \cdots \right.$$
$$\left. + \left\{ \frac{a_1}{G} \right\} \left\{ \frac{a_2 \times A^2 + a_1^2 \times M}{H \times A^2} \right\} \right] \cdots$$
$$+ O \times \left\{ \frac{a_1}{A} \right\}^2 \left\{ \frac{a_1}{G} \right\} \Big\rangle \times \left\{ \left\{ \frac{1}{K} \right\}^2 \left\{ \frac{1}{D} \right\} \right\} \quad (15)$$

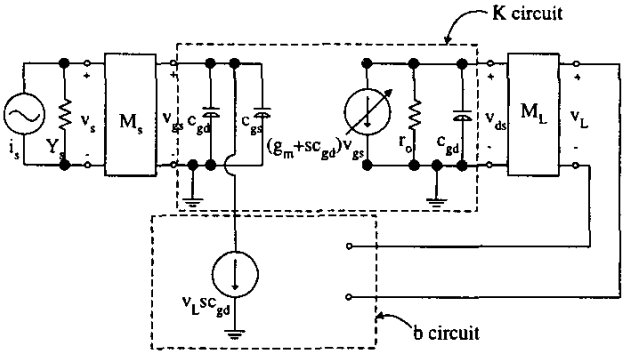

Fig. 2: Shunt-Shunt Feedback Model for Linearity

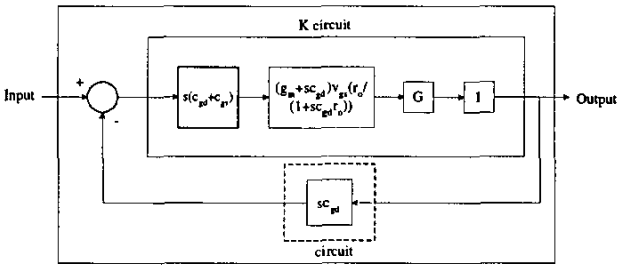

Fig. 3: Closed-Loop Block Diagram for Linearity Feedback System

where

$L = \{2g_2 + j\omega_1 c_2\}$, $M = \{g_2 + j\omega_1 c_2\}$, and $O = \left\{g_3 + \frac{1}{3} j\omega_1 c_3\right\}$.

B. The Effect of Shunt Feedback on Linearity

Next, the effect of C_{gd} on linearity will be developed via a modified small-signal model. We begin by examining Fig. 2 where the small-signal model has been restructured into a shunt-shunt feedback model. The linear feedback comes from C_{gd} and its contribution to the current in the input and output loop circuits has been distributed from the structure of Fig. 1 [8].

The next step is to associate the feedback model in Fig. 2 with the closed-loop block diagram system in Fig. 3 where components can be grouped and divided into linear and nonlinear contributions to the amplifier output. Then the nonlinear analysis of Sec. II.A can be modified to include the effect of linear feedback on the form of the final transfer functions.

The feedback terms of the circuit, β, can be identified from Fig. 3

$$\beta_1(j\omega_1) = \beta_1 = \quad j\omega_1 c_{gd} \quad (16)$$

where

$$\beta_2(j\omega_1, j\omega_2) = 0 \quad (17)$$

where

$$\beta_3(j\omega_1, j\omega_2, j\omega_3) = 0 \quad (18)$$

Next the gain reduction factors are found; i.e.,

$$R(j\omega_1) = \frac{1}{1 + K_1(j\omega_1)\beta_1(j\omega_1)} \tag{19}$$

$$R(3j\omega_1) = \frac{1}{1 + K_1(3j\omega_1)\beta_1(3j\omega_1)} \tag{20}$$

With these definitions, the overall Volterra kernels can be expressed including linear feedback [8].

$$v_{ds} = Q_1 \circ i_s + Q_2 \circ i_s^2 + Q_3 \circ i_s^3 + \cdots \tag{21}$$

where

$$\mathrm{Q_1(j\omega_1)} = \frac{\mathrm{K_1(j\omega_1)}}{[1 + \mathrm{K_1(j\omega_1)\beta(j\omega_1)}]} \tag{22}$$

and

$$Q_2(j\omega_1, j\omega_1) = R(j\omega_1)^2 R(2j\omega_1) K_2(j\omega_1, j\omega_1) \tag{23}$$

and

$$Q_3(j\omega_1, j\omega_1, \ j\omega_1) = R(j\omega_1)^3 \left[K_3(j\omega_1, j\omega_1, \ j\omega_1) \right. \\ \left. \frac{2K_2(j\omega_1, j\omega_1)K_2(j\omega_1, 2j\omega_1)}{K_1(2j\omega_1)}\right] R(3j\omega_1) \tag{24}$$

where

$$\mathrm{K_2(j\omega_1, 2j\omega_1)} = \left[\frac{\{\mathrm{a_1}\}\frac{3}{2}\mathrm{j\omega_1 c_{g_2}} \quad \{\mathrm{a_2}\} + \frac{\mathrm{I_2}}{\mathrm{A*H}})) * \mathrm{F_3}}{\mathrm{A_3 * F_3 * K * E}}\right] \tag{25}$$

where

$\mathrm{A_3} = \{\mathrm{g_1} + \mathrm{y_L}(3\omega_1) + 3\mathrm{j\omega_1 c_1}\}$,
$\mathrm{F_3} = \{\mathrm{y_s}(3\omega_1) + 3\mathrm{j\omega_1 c_{g1}}\}$, and $\mathrm{I_2} = \mathrm{a_1^2}(\mathrm{g_2} + \frac{3}{2}\mathrm{j\omega_1 c_2})$.

$$\mathrm{K_1(2j\omega_1)} = \frac{\mathrm{a_1}}{\mathrm{H * E}} \tag{26}$$

Some expansion and substitution of terms will be required to create the final form of the Volterra Kernels with linear feedback. The following derivation relies on the results of Sec. II.A using the different forms of K_n , where $n = 1, 2, 3$ [9].

The ratio of third order intermodulation distortion to the desired signal, IMD_3 , is given by [5]

$$IMD_3 = \frac{3|Q_3(j\omega_1, j\omega_1, \ j\omega_1)|}{4|Q_1(j\omega_1)|} s_i^2 \tag{27}$$

The third order input intermodulation intercept point, $IIIP_3$, can be computed from the following:

$$IIIP_3 = \frac{IMD_3}{2} + P_\Delta \tag{28}$$

where P_Δ is the input power at the IMD_3 [10].

Using (28) and specific matching conditions, linearity estimates from theory can be made to compare to measured results as a function of bias.

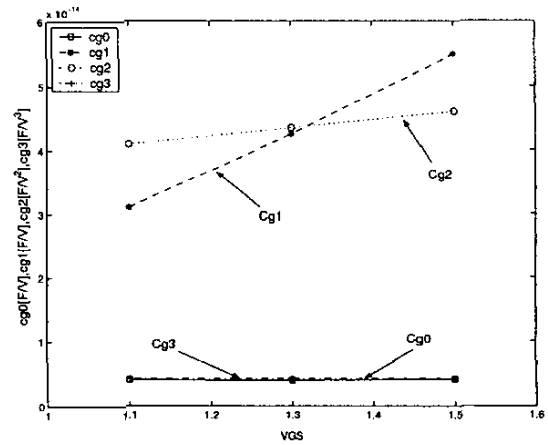

Fig. 4: N50μm x 0.35μm C_{gs} Coefficients vs. VGS at VDS=1.5V

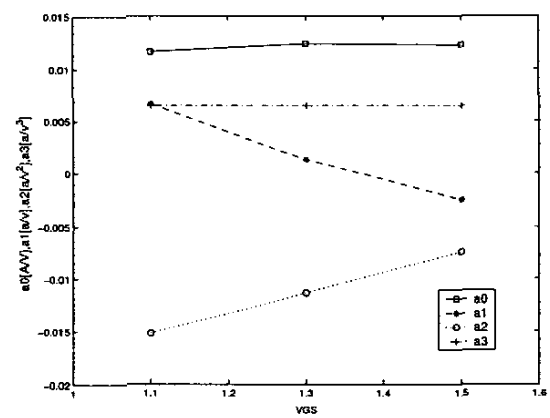

Fig. 5: N50μm x 0.35μm gm Coefficients vs. VGS at VDS=1.5V

III. Experimental Results

The theory described above was verified with 0.35μm gate length NMOS devices at 5 GHz. Coefficients were derived for each of the nonlinear elements described in Sec. II by polynomial expansion and fitting about a large-signal operating point in MatLab based on measured IV curves under specific bias conditions. Thus, the power series expansion given in 1, for instance, contains both the large-signal value of transconductance, a_0, and the small-signal value of transconductance, a_1, along with higher orders, a_n. This provides for prediction of the transconductance in the presence of both large-signal and small-signal excitation. Similar expansions were made for the other nonlinear elements shown in Fig. 1.

Figs. 4 and 5 show the relative sensitivity for each set of coefficients, C_{gs} and g_m, modelling each of these two nonlinear elements given in (4) and (1) as a function of V_{GS}. In both cases, the large-signal values in saturation vary little relative to the first and second order small-signal values as a function of V_{GS}. The third order, small-signal values, such

Table 1: N50μm x 0.35μm Theoretically Predicted vs. Measured IIP_3 dBm at VDS=1.5V

Term. Imped.	Vgs Bias	Mea.	Pred.	Diff.
T(1)	1.1 V	11.1	13.95	2.87
T(2)	1.1 V	8.99	10.68	1.69
T(3)	1.1 V	9.04	10.38	1.34
T(4)	1.3 V	12.2	15.86	3.65
T(5)	1.3 V	12.5	16.44	3.9
T(6)	1.3 V	12.6	14.68	2.12
T(7)	1.5 V	14.73	15.45	0.72
T(8)	1.5 V	14.71	14.83	0.12
T(9)	1.5 V	13.44	12.44	0.998

Table 2: N50μm x 0.35μm Load Terminating Impedances for Measured IIP_3

Term. Imped.	$\lvert \Gamma_1 \rvert$	$\angle \Gamma_1^\circ$	$\lvert \Gamma_2 \rvert$	$\angle \Gamma_2^\circ$	$\lvert \Gamma_3 \rvert$	$\angle \Gamma_3^\circ$
$T_L(1)$	0.647	258.6	0.815	239	0.806	64.8
$T_L(2)$	0.647	258.6	0.815	239	0.806	64.8
$T_L(3)$	0.28	256.4	0.466	180.4	0.484	322.6
$T_L(4)$	0.685	217.6	0.849	166.5	0.878	323.7
$T_L(5)$	0.320	314.3	0.801	3.3	0.822	251.3
$T_L(6)$	0.632	314.3	0.801	3.3	0.822	251.3
$T_L(7)$	0.563	85.8	0.810	281.7	0.841	310.7
$T_L(8)$	0.653	154.3	0.853	51.9	0.839	149.7
$T_L(9)$	0.559	341.8	0.751	60.3	0.783	332.0

Table 3: N50μm x 0.35μm Source Terminating Impedances for Measured IIP_3

Term. Imped.	$\lvert \Gamma_1 \rvert$	$\angle \Gamma_1^\circ$	$\lvert \Gamma_2 \rvert$	$\angle \Gamma_2^\circ$	$\lvert \Gamma_3 \rvert$	$\angle \Gamma_3^\circ$
$T_S(1)$	0.465	199.6	0.704	31.6	0.733	280.6
$T_S(2)$	0.688	178.1	0.867	11.6	0.881	262.2
$T_S(3)$	0.668	178.1	0.867	11.6	0.881	262.2
$T_S(4)$	0.410	231.7	0.639	90.4	0.648	7.7
$T_S(5)$	0.410	231.7	0.639	90.4	0.648	7.7
$T_S(6)$	0.660	146.3	0.864	310.5	0.894	175.5
$T_S(7)$	0.335	195.8	0.561	12.8	0.609	247.0
$T_S(8)$	0.335	195.8	0.561	12.8	0.609	247.0
$T_S(9)$	0.495	179.0	0.751	60.3	0.778	228.7

as, a_3, also vary little as a function of V_{GS}. As an example, Table 1 shows the agreement between predicted IIP_3 and measurements, and the data agrees to within an average 1.9 dBm across differing bias and matching conditions. The many source and load matching impedance terms and their harmonics necessary for the IMD_3 prediction are shown in Tables 2 and 3. Table 2 shows the load matching impedance terms and harmonics of the load matching terms. Table 3 shows the source matching impedance terms and harmonics of the source matching terms.

The measurements were conducted at wafer level using a Focus Microwaves passive load-pull system at a bias of VDS=1.5V at 21° C. These result can be used to predict the linearity of a common-source amplifier at any bias and terminating impedance.

As a final note, for which further explanation and data will be delivered in future research reports, is the interaction in the theoretical prediction of intermodulation between the nonlinear modelling terms and the matching and harmonics of matching terms as the dominant effect in determining the quality of the intermodulation prediction. In other words, matching in RF circuit is highly significant for intermodulation characterization and performance.

IV. Conclusions

A Volterra series analysis of a MOSFET common-source amplifier has been done, which allows us to predict the linearity as a function of bias and terminating impedance. Experimental results verify the utility of the technique.

V. Acknowledgement

The authors gratefully acknowledge the support of the Army Research Office MURI Program "Digital Communications Devices Based on Nonlinear Dynamics and Chaos," under the direction of Dr. John Lavery.

VI. References

[1] D. Shaeffer and T. Lee, "A 1.5V, 1.5-GHz CMOS Low Noise Amplifier," *IEEE Journal of Solid-State Circuits*, vol. 32, pp. 745–750, May 1997.

[2] L. Larson, "Integrated Circuit Technology Options for RFIC's–Present Status and Future Directions," *IEEE Journal of Solid-State Circuits*, vol. 33, pp. 387–399, Mar. 1998.

[3] B. Razavi, "CMOS Technology Characterization for Analog and RF Design," *IEEE Journal of Solid-State Circuits*, vol. 34, pp. 268–276, Mar. 1999.

[4] C. Feng *et al.*, "Analysis of Nonlinearities in RF CMOS Amplifiers," *Proceedings of ICECS '99. 6th IEEE International Conference on Electronics, Circuits and Systems*, vol. 1, pp. 137–140, 1999.

[5] D. Weiner and J. Spina, *Sinusoidal Analysis and Modeling of Weakly Nonlinear Circuits*. Van Nostrand Reinhold, 1980.

[6] K. Fong and R. Meyer, "High-Frequency Nonlinear Analysis of Common-Emitter and Differential-Pair Transconductance Stages," *IEEE Journal of Solid-State Circuits*, vol. 33, pp. 548–549, Apr. 1998.

[7] Y. Tsividis, *Operation and Modeling of the MOS Transistor*. McGraw Hill, 1999.

[8] P. Wambacq and other, *Distortion Analysis of Analog Integrated Circuits*. Kluwer Academic, 1998.

[9] S. Maas, *Nonlinear Microwave Circuits*. IEEE Press, 1997.

[10] R. Carson, *Radio Communications Concepts: Analog*. John Wiley and Sons, 1990.